

Gamma ray and Neutrinos fluxes from a cosmological dark matter simulation

E. Athanassoula¹, F.-S. Ling², E. Nezri^{1,2}, R. Teyssier³

¹*Laboratoire d'Astrophysique de Marseille,
Observatoire Astronomique de Marseille Provence
CNRS/Université de Provence
2 Place Le Verrier, 13248 Marseille Cédex 04, France*

²*Service de Physique Théorique, Université Libre de Bruxelles,
CP225, Bld du Triomphe, 1050 Brussels, Belgium*

³*DAPNIA, CEA Saclay
L'Orme des merisiers 91191 Gif-sur-Yvette, France*

Abstract

In this paper, we estimate the gamma-ray and neutrino fluxes coming from dark matter annihilation in a Milky Way framework provided by a recent N-BODY HORIZON simulation. We first study the characteristics of the simulation and highlight the mass distribution within the galactic halo. The general dark matter density has a typical r^{-3} power law for large radii, but the inner behaviour is poorly constrained below the resolution of the simulation (~ 200 pc). We identify clumps and subclumps and analyze their distribution, as well as their internal structure. Inside the clumps, the power law is rather universal, $r^{-2.5}$ in the outer part with again strong uncertainties for smaller radii, especially for light clumps. We show a full-sky map of the astrophysical contribution to the gamma-ray or neutrino fluxes in this N-body framework. Using quite model independent and general assumptions for the high energy physics part, we evaluate the possible absolute fluxes and show some benchmark regions for the experiments GLAST, EGRET, and a km³ size extension of ANTARES like the KM3NeT project. While individual clumps seem to be beyond detection reach, the galactic center region is promising and GLAST could be sensitive to the geometry and the structure of its dark matter distribution. The detection by a km³ version of ANTARES is, however, more challenging due to a higher energy threshold. We also point out that the lack of resolution leaves the inner structure of subhalos poorly constrained. Using the same clump spectrum and mass fraction, a clump luminosity boost of order ten can be achieved with a steeper profile in the inner part of the sub-halos.

1 Introduction

An ever increasing number of observational and theoretical results strongly suggest, or even require the existence of dark matter, whose enigma becomes thus crucial for the understanding of our universe. Let us mention amongst others the WMAP results on CMB [1], the rotation curves of disk galaxies [2], the formation of large scale structures [3], the bullet cluster observation [4], merger modeling and lensing results *e.g.* [5]. Finally, the possibility of numerous extensions of high energy physics beyond the standard model (BSM) to provide new weakly interacting massive particle (WIMP) candidates for dark matter makes the hypothesis very appealing.

Nevertheless, the nature, the identification and the distribution of the dark matter are still open questions, intimately linked with the proof of its existence. Present and near future instrumental projects could bring welcome input to these questions. Namely, both astroparticle physics and collider searches will reach higher sensitivities with experiments like LHC (accelerator); EDELWEISS II, superCDMS and ZEPLIN (direct detection); ANTARES and ICECUBE (neutrino telescopes); GLAST (gamma space telescope) and PAMELA (charged particle search satellite). Amongst the different possibilities, indirect detection is particularly promising. Indeed, relic dark matter particles can accumulate in cosmic storage rings and annihilate. The decay of their annihilation products will give rise to secondary particle fluxes ($\gamma, \nu, e^+, \bar{p}$), which could be detected by dedicated experiments indirectly indicating the presence of dark matter.

In this paper, we will focus on indirect detection of dark matter through gamma rays and neutrinos. Galaxies are thought to be interesting sources for this kind of detection, seen the amount of dark matter they are believed to harbour. As we will discuss later, the detectability of such gamma rays or neutrinos depends strongly on both the astrophysical assumptions on the dark matter distribution in the halo and on the assumed high energy physics BSM scenario. Some studies concerning different particle physics models can be found in the literature (see [6, 7] for reviews). The popular BSM dark matter scenarios are typically supersymmetric models, models with extra dimensions, light dark matter, little Higgs model, inert doublet model ... or any extensions providing WIMP. The Milky Way astrophysical framework is commonly simplified with assumptions of spherical symmetry, now known to be incorrect [8, 9, 10, 11], and typical smooth dark matter density functions extracted from N-body simulations [12, 13, 14]. Few recent works [15, 16, 17] and especially [18] with an impressive resolution treat in detail the astrophysical aspects of the gamma ray fluxes coming from dark matter annihilation in realistic simulation frameworks. Other works *e.g* [19, 20, 21, 22, 23] consider also more sophisticated parametrization inspired by extrapolations of simulation results.

Typical simulation canvas consist of 1-100 millions of particles with mass around $10^5 - 10^6$ solar masses. The results reproduce well the large-scale structure formation and have now shown that virialized systems are still left with surviving subhalos, also called *clumps*. The results are more and more promising with computing upgrades and resolution improvements. Nevertheless, some questions are still open with regard to observations. For instance, the radial density profiles predicted for the innermost region of galactic halos are quite cuspy, whereas observations suggest flat cores (see [2] for a review). Furthermore, simulations predict more numerous galactic satellites than observed for the Milky Way. Even if N-body calculations may generate too concentrated objects, the simulated haloes are the only realistic or advanced dark matter distribution framework. Specifically, the estimation of dark matter detectability in our neighborhood depends on both the dark matter distribution in the Milky Way – especially in the innermost region – and on the number, the size and the concentration of the clumps. Depending on the assumptions or results on these key points, different results have been proposed in previous works [21, 24, 25, 26, 27, 22, 28, 29, 23, 30].

The present article is devoted mainly to the astrophysical contribution concerning dark matter gamma and neutrino indirect detection. We calculated the possible gamma and neutrino fluxes sky map in a N-body simulation framework provided by a HORIZON project simulation [31]. The paper is organized as follows: section 2 gives the analysis of the numerical simulation and highlights the resulting dark matter distribution. In section 3, the gamma ray and neutrino flux calculation is shortly reviewed and a comparison of our estimates with regard to GLAST and ANTARES reach is presented. Conclusion and perspectives are given in section 4.

2 Simulation characteristics

2.1 General features

The data used for this paper were provided by the Horizon collaboration. The simulation was performed using the Adaptive Mesh Refinement code RAMSES [32]. The initial conditions are set by the WMAP3 results ($\Omega_m = 0.24$, $\Omega_\Lambda = 0.76$, $\Omega_b = 0.042$, $n = 0.958$, $H_0 = 73$, $\sigma_8 = 0.77$) and the effective number of particles is $N_p = 1024^3$ in a box of size $L = 20h^{-1}$ Mpc. At $z = 0$ we selected a Milky-Way sized halo. Using the so-called “zoom” technique, we re-defined the grid outside a sphere of diameter $5h^{-1}$,

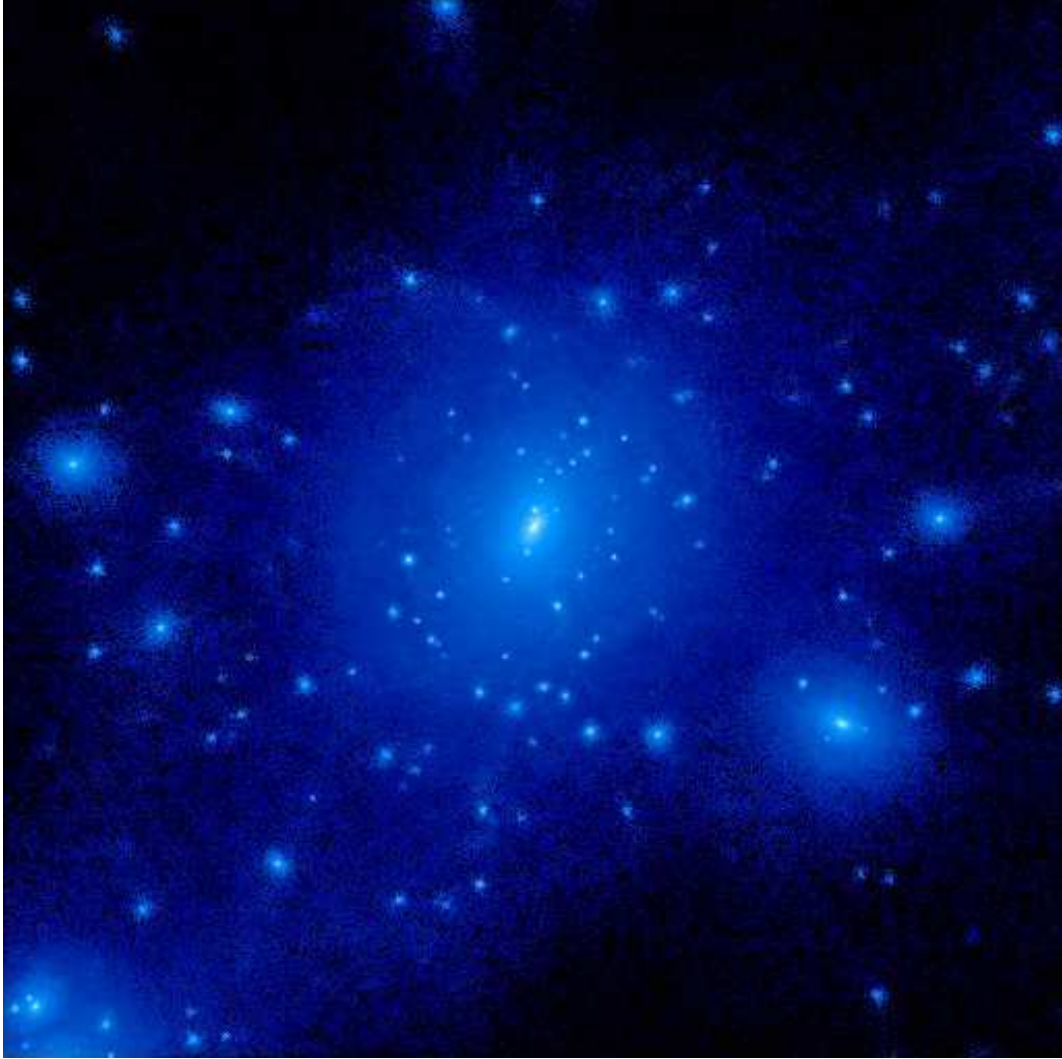


Figure 1: View of the galactic dark matter halo in the HORIZON simulation (projected along the z axis). The box size corresponds to 750 kpc.

using high-mass particles to sample the large scale tidal field and smaller ones for the selected halo region. In the high-resolution region, we increase the resolution of the grid on a cell-by-cell basis, with a maximum of 7 additional levels of refinement, corresponding to a maximum linear resolution of about 200 pc. Cells are refined if the local number of dark matter particles exceeds 10. Our smallest particle mass is $M_p = 7.46 \cdot 10^5$ in solar mass (M_{sun}) units. Our simulated galactic environment is depicted in Fig. 1.

The size of a galactic halo is characterized by its virial radius, r_{vir} , often defined as the size of the sphere centered on the galaxy center with an average density equal to 200 times the cosmological matter density. In our simulation, the virial radius is equal to 253 kpc, corresponding to an enclosed mass of $6.05 \times 10^{11} M_\odot$ or 8.1×10^5 particles.

Dark matter halos are often parameterized by spherically symmetric profiles of the form

$$\rho(r) = \rho_0 \left(\frac{r}{r_0} \right)^{-\gamma} \left[\frac{1 + (r_0/a)^\alpha}{1 + (r/a)^\alpha} \right]^{\frac{\beta-\gamma}{\alpha}}, \quad (1)$$

where ρ_0 is the local density in the solar neighborhood, $r_0 = 8$ kpc is the distance from the sun to the

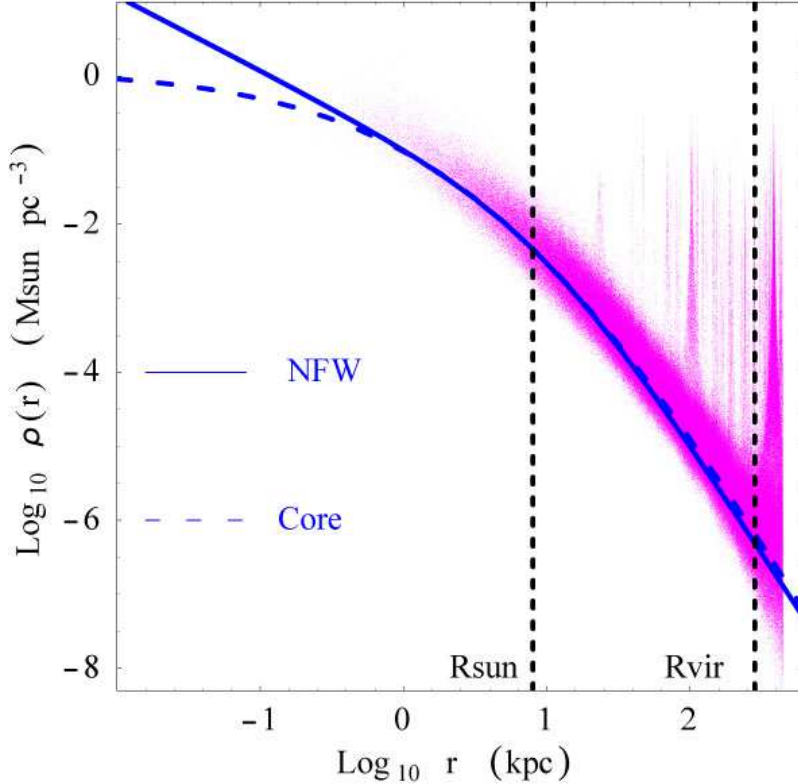


Figure 2: Density at all the positions of the particles in the simulation as a function of their distance to the center. This is compared to NFW ($\alpha = 1$, $\beta = 3$ and $\gamma = 1$, $a = 10$ kpc, solid line) and core ($\alpha = 0.5$, $\beta = 3.3$, $\gamma = 0$, $a = 4.5$ kpc, dashed line) profiles.

galactic centre, γ is the inner slope, β is the outer slope. α describes the transition behavior around $r = a$. The popular NFW profile [12] has $\alpha = 1$, $\beta = 3$ and $\gamma = 1$ and, adapted to the Milky Way, corresponds to $a = 20$ kpc and $r_0 = 8$ kpc.

Fig. 2 depicts the radial distribution of the density for all particles in our simulation, calculated by the method of Casertano and Hut [33], as will be discussed below. The center is taken as the densest point of the galactic halo. Due to resolution limits, this distribution is globally consistent both with a NFW-like profile ($\alpha = 1$, $\beta = 3$ and $\gamma = 1$, $a = 10$ kpc) and a cored profile ($\alpha = 0.5$, $\beta = 3.3$, $\gamma = 0$, $a = 4.5$ kpc), with $r_0 = R_{sun} = 8$ kpc in both cases. At any given radius, the densities exhibit a large spread due to non sphericities, local fluctuations and also statistical biases. Moreover, numerous density peaks from substructures are also apparent. Notice that the best fit profile is given by the set of parameters ($\alpha = 0.39$, $\beta = 3.72$, $\gamma = 0.254$, and $a = 13.16$ kpc), but its physical significance is arguable, given the large density fluctuations aforementioned.

As there is no baryonic component in this simulation, the sun location can be chosen in any direction. For the full skymap pictures in the next section, two positions were chosen, one along the positive z axis (which is also the projection axis in Figs. 1 and 3) and one along the positive x axis. The corresponding dark matter densities coincide to within 10% and are $\rho_0 = 0.0046 M_{\odot}\text{pc}^{-3} = 0.17 \text{ GeVcm}^{-3}$ and $\rho_0 = 0.0043 M_{\odot}\text{pc}^{-3} = 0.165 \text{ GeVcm}^{-3}$ respectively. Throughout the rest of the paper, we will use the former for normalization purposes.

The density around a simulation point i was calculated with the algorithm of Casertano and Hut [33], namely

$$\rho_j^i = \frac{j-1}{V(r_j)} M_p \quad (2)$$

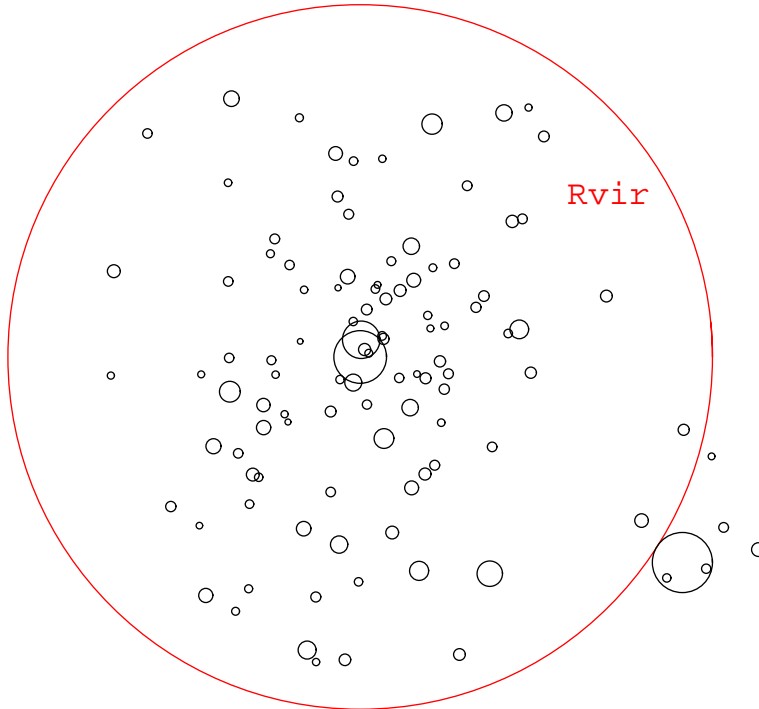


Figure 3: Clump distribution in the galaxy, projected along the z axis. The location of each clump is identified by a circle, whose size scales as $M^{1/3}$. The red (largest) circle shows the virial radius (as defined in the text) of the galaxy (253 kpc).

where $V(r_j) = 4\pi/3r_j^3$ is the volume of the smallest sphere around the particle i that includes j neighbors. Excluding the particle i itself as well as the j th neighbor in the mass count gives an unbiased estimator of the density, with a variance $\sigma_j^2 = \rho^2/(j-2)$. The choice of the number of neighbors used to calculate the density is a trade-off between reducing fluctuations and preserving the locality of the value computed by this method. A value $j \simeq 10$ seems to give a satisfactory compromise, as we could check on some Plummer test models. Higher values of j wash out substructures and inhomogeneities present in the data, while smaller values of j imply large statistical uncertainties that mask these inhomogeneities with Poissonian noise. As can be seen in Fig. 2, the density inside clumps can be several orders of magnitude higher than the density of the smooth component at that location.

2.2 Clumps

To identify clumps and subclumps in our simulation, we used the code ADAPTAHOP [34], which is an improved algorithm based on HOP that enables to build a tree of structures and substructures. Basically, the algorithm divides the simulation points into disconnected groups, or leaves, corresponding to local density maxima. To decrease statistical noise, smoothing techniques are applied to calculate the density. The connections between leaves are created by performing a search of saddle points between groups. The density of a saddle point is then compared with the local maxima on each side, as well as a threshold parameter, to decide whether the structures are connected or not. By progressively raising this threshold from a minimum value corresponding to a galactic halo overdensity, and performing recursively the last check, the algorithm constructs a tree of (sub)structures. We note that the peak patches output by ADAPTAHOP are disconnected in space, as they are limited by the closest saddle points. As a consequence, clump masses given by this algorithm are often underestimated if other structures are present in their neighborhood. We found 108 (sub)clumps attached to the galaxy. Their

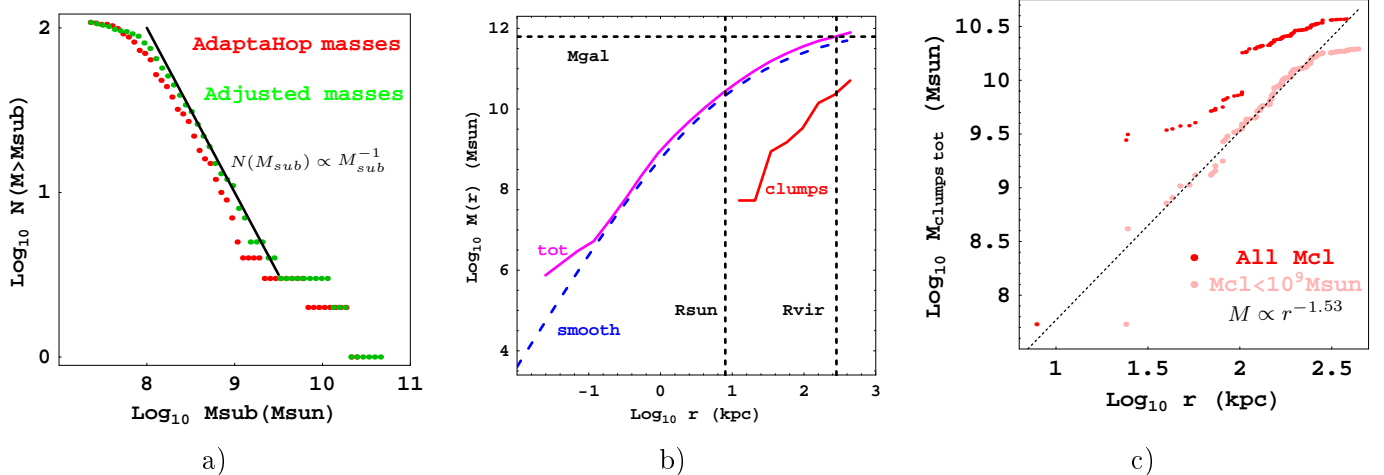


Figure 4: a) Cumulative subhalo mass function of the clumps in the galaxy obtained with ADAPTAHOP masses (red - dark grey) and after the virial mass adjustment procedure (green - lighter grey). b) Cumulative mass for the simulation (tot), the smooth component and the clumps. c) A closer look at the cumulative mass profile for the clumps (all clumps in red, and only clumps lighter than $10^9 M_{\odot}$ in pink).

spatial distribution is illustrated in Fig. 3, where each clump is represented by a circle whose radius scales as the $1/3$ power of its mass, $M^{1/3}$. A comparison with Fig. 1 shows that the two pictures are consistent. All the clumps within the virial radius are successfully identified by the algorithm. Outside this radius, some clumps are found as disconnected from the main galaxy, and therefore not visible on Fig. 3.

From this, we derived a cumulative subhalo mass function shown on Fig. 4a. The clumps mass fraction inside the virial radius is equal to 3.6% of the total mass within that radius when taking the mass values output by ADAPTAHOP. We have corrected these masses by fitting a density profile on each clump, and then extrapolating it to the clump virial radius. The adjusted clumps mass fraction inside the virial radius is then equal to 5.4%. The mass adjustment has an impact on the mass function, as can be seen on Fig. 4a. The result is compatible with a power-law with index -1 above a mass threshold of $5 \times 10^8 M_{\odot}$. For smaller masses, a flattening of the curve is apparent, due to the resolution limit of the simulation, which does not allow the survival of clumps with mass below a given threshold. This is around 200 particles, in agreement with [16]. The effect of the mass adjustment further enhances this flattening at low masses. Even after this correction, the final mass function that we get is still lower than that found by other authors [15, 16], but this deviation is not statistically significant. For example, we found 3 (7) clumps with mass before (after) adjustment higher than $10^9 M_{\odot}$, compared to 13 in [16].

For the clump radial number density distribution, the statistics is too low to obtain reliable information about the behavior near the galactic center (GC). Instead, it is preferable to look at the cumulative mass profile as a function of the radius (distance from the GC), shown on Fig. 4b and c. When the clumps with a mass $> 10^9 M_{\odot}$ are removed, the cumulative mass profile is well fit by a power-law with index $n \simeq 1.75$ up to the virial radius. The corresponding clump mass density profile with index $n - 3 \simeq -1.25$ is thus flatter than the smooth component. The mass fraction in the form of clumps is therefore increasing with radius. This can be intuitively understood, since clump merging should be easier in the central parts. However, the clump density in this simulation is too low to dominate the mass fraction at any radius up to the virial radius.

Examples of density profiles within two clumps are given in Fig. 5. Except for the inner parts, they are compatible with a power law with slope $\simeq -2.5$ (Fig.5). It is clear that further in there is a sharp transition, but we do not have sufficient points to constrain the inner slopes. In Fig. 5 we have, as an illustration, plotted two power laws with slopes 0 and 1, respectively. The transition between the outer

slope and the inner slope is described by a concentration parameter $c_{vir} = r_{vir}^{cl}/r_{-2}$, where r_{-2} is the radius at which $d/dr (r^2\rho(r)) = 0$ and r_{vir}^{cl} is the virial radius of the clump. Several models predict that the concentration parameter strongly correlates with the virial mass (figure 2 of [23]).

3 Gamma and neutrino fluxes from dark matter annihilation

In this work, we consider that the dark matter particle candidate is a typical WIMP provided by some new physics beyond the standard model. The gamma ray or neutrino flux per solid angle unit from the annihilation of dark matter particles (with mass m_{DM} , density ρ_{DM} , cross-section $\langle\sigma v\rangle$, and branching ratios BR_i into final state i) can be written as

$$\frac{d\Phi_{\gamma,\nu}}{d\Omega} = \frac{1}{4\pi} \underbrace{\frac{1}{\delta} \frac{\langle\sigma v\rangle}{m_{DM}^2} \int_{E_{min}^{\gamma,\nu}}^{E_{max}^{\gamma,\nu}} \sum_i \frac{dN_{\gamma,\nu}^i}{dE_{\gamma,\nu}} BR_i}_{\doteq HEP_{\gamma,\nu}} \underbrace{\int_{l(\vec{\Omega})} \rho_{DM}^2 dl}_{\doteq ASTRO} , \quad (3)$$

where $dN_{\gamma,\nu}^i/dE_{\gamma,\nu}$ is the differential gamma/neutrino spectrum per annihilation coming from the decay of annihilation products of final state i , the integral is taken along the line of sight with direction $\vec{\Omega}$, and $\delta = 2$ for a self conjugate dark matter particle and 4 otherwise. We have separated into two brackets factors that arise from particle physics and from astrophysics.

The annihilation signal is proportional to the density squared, and can therefore benefit from a strong enhancement if the dark matter distribution is highly clumpy. This enhancement is known as the *boost factor*.

3.1 Astrophysics factor

To further discuss the enhancement due to the distribution, it is useful to define the dimensionless quantity

$$\bar{J}(\Delta\Omega) = \frac{1}{\Delta\Omega} \frac{1}{\rho_0^2 r_0} \int \rho^2 dl d\Omega, \quad (4)$$

where the solid angle $\Delta\Omega$ can be taken as the experimental solid angle resolution of a given experiment such as GLAST.

To evaluate this quantity for our simulation, two different methods can be used. In the first method, ρ^2 can be calculated at any coordinate of the simulation box space with the Casertano-Hut algorithm. Note that the estimator of ρ^2 is smaller than the square of the estimator for ρ by a factor $(j-2)/(j-1)$. The integral along a given line of sight is then calculated with the method of rectangles, with a variable step equal to half of the distance to the $j = 10$ th closest neighbor. This ensures that the integral will not be overestimated when local density peaks are encountered along the line of sight. Finally, the value of \bar{J} in a cone is the average of the values for different lines of sight within that cone. Fig. 6 presents an all-sky view of the astrophysical factor \bar{J} in a Hammer projection for a value $\Delta\Omega = 10^{-5}$ relevant for GLAST. Since the simulation does not include a baryonic component, the position of the observed is only constrained by its distance from the center, i.e. can be anywhere on a sphere of radius 8 kpc. We calculated the \bar{J} all sky map for two different viewing positions to allow comparisons. The shape of the iso- \bar{J} contours differs significantly between the two cases and is not circular-like. Indeed cosmological simulations show that dark matter halos are not spherical, but have the shape of triaxial ellipsoids (e.g. [35, 36]) and this is true also for the simulation we analyze here. Thus, the observed signal will depend on the viewing angle, since the integral in Eq. (4) will have different values if the integration is e.g. along a major or a minor axis of the ellipsoidal shape. This is also noted in the zoom of the central region, shown in Fig. 7. In this figure we also see that the relevant size of the central region is of the order of a kpc, which has been found by galactic dynamic simulations to have a rich structure in the baryonic component, including inner bars, inner discs, rings and/or spirals. Whether these influence in any way the dark matter in that region still remains to be studied.

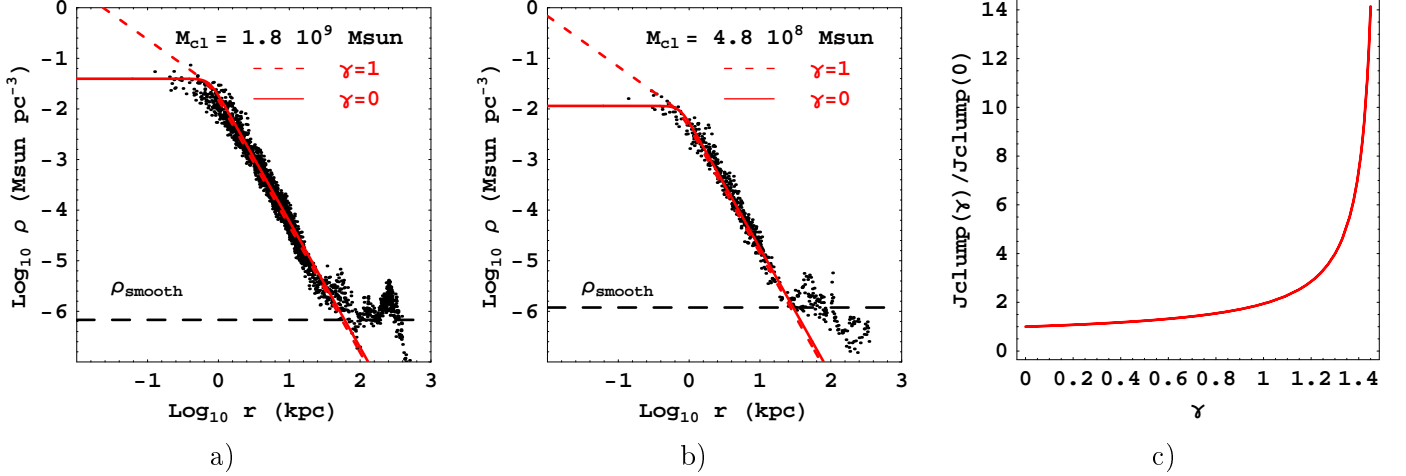


Figure 5: a) and b) Density profile inside two clumps. The outer slope of the profile corresponds to $\beta = 2.5$. c) Clump luminosity boost factor as a function of the exponent of the clump inner density profile (γ).

We also evaluated the astrophysical factor with a second method, in which the integral in Eq. (4) is replaced by a finite sum over simulation points.

$$\hat{J}(\Delta\Omega) = \frac{1}{\Delta\Omega} \frac{1}{\rho_0^2 r_0} \sum_{i \in \Delta\Omega} \frac{\rho_i M_p}{l_i^2} \quad (5)$$

The presence of a pole in l^{-2} is potentially dangerous in this method, and can lead to an overestimation of the fluxes in case a simulation point is very close to the observer's location. Nevertheless for this simulation and for the chosen sun locations, we get comparable results for the two methods, although fluxes from low density regions suffer more from statistical noise. To compare the two numerical methods more globally, we calculated \bar{J} and \hat{J} for the whole sky, $\Delta\Omega = 4\pi$. We found a good agreement ($\sim 2\%$) between the two methods.

3.2 Particle Physics factor

The evaluation of the particle physics contribution ($HEP_{\gamma,\nu}$) in Eq. (3) is highly dependent on the physics beyond the standard model that one assumes. Let us rewrite the HEP term as

$$HEP_{\gamma,\nu} = \frac{1}{\delta} \frac{\langle \sigma v \rangle}{m_{DM}^2} N_{\gamma,\nu} \quad , \quad (6)$$

where $N_{\gamma,\nu}$ is the number of photons/neutrinos per annihilation

$$N_{\gamma,\nu} = \int_{E_{min}^{\gamma,\nu}}^{E_{max}^{\gamma,\nu}} \sum_i \frac{dN_{\gamma,\nu}^i}{dE_{\gamma,\nu}} BR_i \quad . \quad (7)$$

The spectra coming from dark matter particles annihilation spread up to m_{DM} . The number of photons/neutrinos depends on the decay chain of the dark matter annihilation products and these annihilations are determined by the particular particle physics model considered. We can estimate this number by using an effective and quite model independent approach. Namely, we will assume, as in typical BSM model, that dark matter particles (like those coming from SUSY, extra-dimensions ...) annihilate into SM (Standard Model) particles (W^+W^- , $\tau^+\tau^-$, $b\bar{b}$, $t\bar{t}$...) whose decays will, in turn, produce the gamma/neutrino continuum. The spectrum can then be evaluated from Pythia [37] simulations.

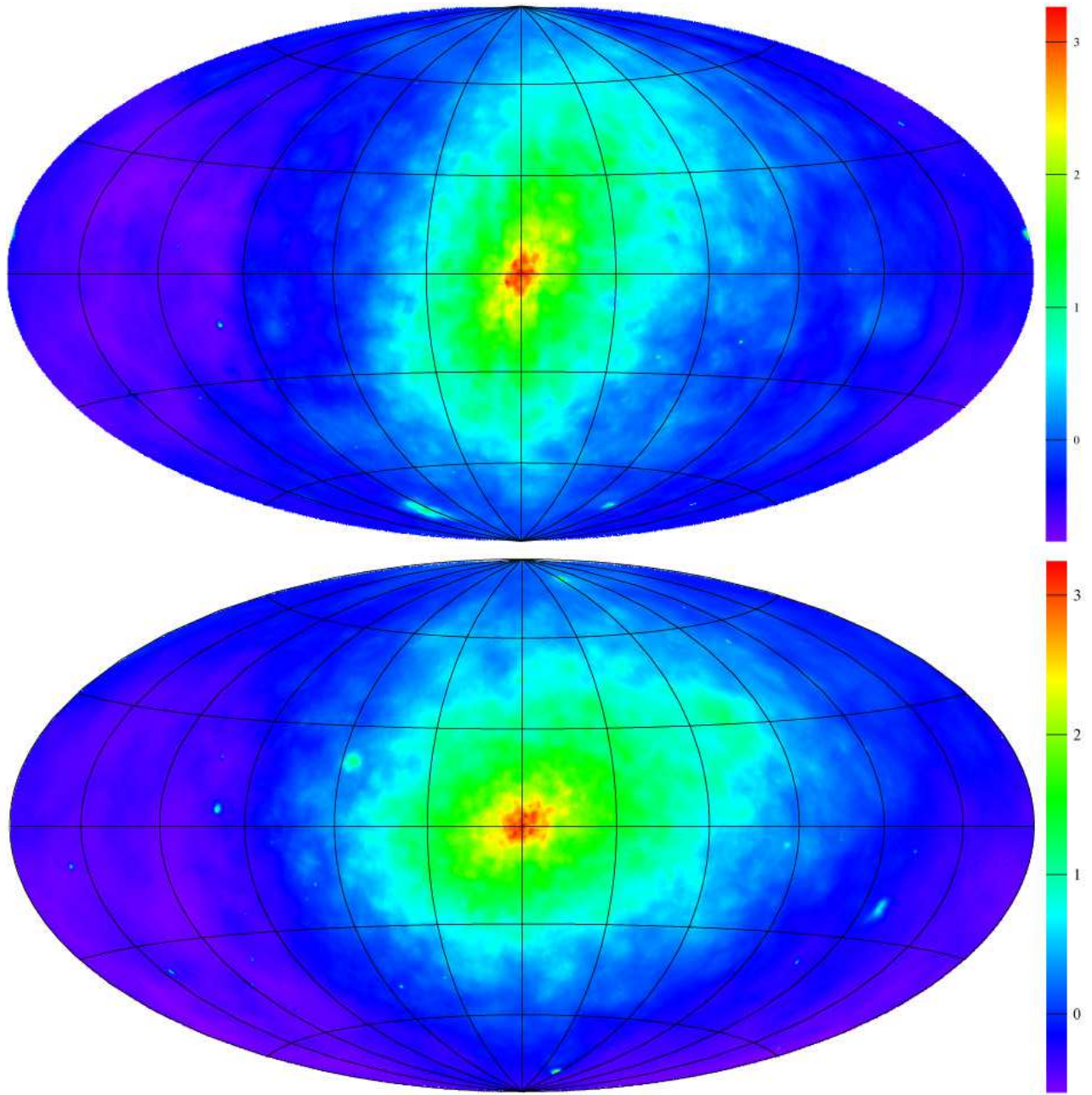


Figure 6: \bar{J} all sky map in a Hammer projection. The observer positions are $(0, 0, R_{sun})$ (top figure) and $(R_{sun}, 0, 0)$ (bottom figure). The values range from less than 1 in the anticenter to more than 10^3 in the direction of the center.

For gamma rays, the actual number of photons in a given experiment depends on its energy range. For GLAST, the energy range will be $\approx 1 - 300$ GeV. These threshold values fix the actual limits for E_{min}^γ and E_{max}^γ . In the 1-300 GeV GLAST energy range, the number of photons estimated from Pythia simulations [38] typically yields $N_\gamma \sim 1, 10, 50$ and 200 for $m_{DM} \sim 10, 100, 1000$ GeV and 10 TeV respectively.

For neutrinos, we will consider the ANTARES sensitivity and a possible improvement for a km3 size telescope located in the mediterranean sea. The typical energy threshold for such a neutrino telescope is ~ 100 GeV leading to $1 \lesssim N_\nu \lesssim 10$ for $100 \text{ GeV} \lesssim m_{DM} \lesssim 10^4 \text{ GeV}$ (derived from Pythia neutrino spectrum [39]).

The other important quantity in Eq. (6) is the annihilation rate $\langle\sigma v\rangle$. From the cosmological point of view, $\langle\sigma v\rangle$ can be related to the relic abundance of dark matter, roughly $\Omega_{DM} \sim 1/\langle\sigma v\rangle$, even if strictly speaking the temperature is higher in the primordial plasma at the freeze-out than in the surrounding sky at the present epoch and $\langle\sigma v\rangle_{T_0} \neq \langle\sigma v\rangle_{freeze-out}$. For a standard annihilation scenario with thermal freeze-out, a value of Ω_{DM} like what was found by WMAP implies $\langle\sigma v\rangle \sim 10^{-26} \text{ cm}^3\text{s}^{-1}$. Of course, different hypotheses can lead to variations in this value. For instance, one can consider some models where coannihilations drive the number of relic particles. Moreover, cosmological scenarios with low reheating temperature could allow to decrease the annihilation cross section and still satisfy the WMAP constraint. Conversely, scenarios with dark matter particle production through late decays (out of equilibrium) of heavier particles could lead to a higher annihilation cross section to respect the WMAP relic density. Considering those sources of variability, almost independently of any specific particle physics framework, we will assume the reasonable range $10^{-27} \lesssim \langle\sigma v\rangle[\text{cm}^3.\text{s}^{-1}] \lesssim 10^{-24}$.

Consequently, taking into account the production of photons and neutrinos and the annihilation rate uncertainties, a typical range for the HEP contribution to the gamma and neutrinos fluxes are given by

$$10^{-33} \lesssim HEP_\gamma [\text{photons cm}^3.\text{s}^{-1}.\text{GeV}^{-2}] \lesssim 10^{-26} \quad , \quad (8)$$

$$10^{-34} \lesssim HEP_\nu [\text{neutrinos cm}^3.\text{s}^{-1}.\text{GeV}^{-2}] \lesssim 10^{-28} \quad , \quad (9)$$

where the difference between gamma and neutrino is due to the higher energy threshold in neutrino experiments, which reduces N_ν and leads to consider higher values of the dark matter mass ¹.

3.3 Comparison with experiments

With typical values for the local dark matter density $\rho_0 \simeq 0.3 \text{ GeVcm}^{-3}$ [41] and for the Sun to Galactic Center distance $r_0 \simeq 8 \text{ kpc}$, one has

$$\Phi_{\gamma,\nu} [\text{photons/neutrinos cm}^{-2}.\text{s}^{-1}] \sim 10^{20} HEP_{\gamma,\nu} \bar{J} \Delta\Omega. \quad (10)$$

3.3.1 GLAST

GLAST [42] is a satellite which should be launched this year. Its angular resolution should be $\Delta\Omega \sim 10^{-5} \text{ srad}$ (*i.e.* an opening angle of 0.1 degrees). Considering the sky sensitivity of GLAST given by [43], we take $10^{-10} \text{ photons cm}^{-2}\text{s}^{-1}$ as a reasonable value to determine the interesting benchmark region in excess of which we could expect a signal to be detected by GLAST.

In Fig. 7, we show a zoom of the central region of Fig. 6 for the two viewing angles analyzed. The image size is $60 \text{ deg} \times 60 \text{ deg}$. To smooth the artificial substructures that are due to noise in the simulation, we averaged the fluxes in a $5 \times 5 = 25$ pixels square that corresponds to a linear resolution of 200 pc. Taking into account the HEP_γ contribution, we indicate the \bar{J} values of 10^3 and 10^2 as quite optimistic GLAST benchmarks. The two figures show \bar{J} values normalized with the *same* local density. One has to keep in mind that the local density can well vary by an order of magnitude depending on the Sun location (see Fig. 2) and that this will influence accordingly the calculated flux value.

¹This gives typically 2-3 orders of magnitude between EGRET and ANTARES performances despite their similar sensitivities ($\sim 10^{-8-7} \gamma(\nu) \text{ cm}^{-2}\text{s}^{-1}$). The same is true for explicit SUSY models [40].

3.3.2 ANTARES and a km3 size neutrino telescope

AMANDA and ICECUBE are located at the south pole, so that the galactic center region, which is the most promising one, is very challenging for those experiments. Thus, we consider in this section the ANTARES experiment, whose deployment completion is imminent, and extrapolate the sensitivity for a possible km3 size neutrino telescope in the mediterranean sea like the KM3NeT project [44] associating ANTARES, NEMO and NESTOR collaborations. The resolution of Antares depends on the neutrino-muon angle, but is typically $\Delta\Omega \sim 10^{-3}$ sr. We consider the galactic center sensitivity of ANTARES for dark matter derived in [45], the recent improvement of effective area due to trigger update [46] and the expected performance for a km3 size telescope [44]. Taking those references into account, we believe that the sensitivity above 100 GeV of a future km3 size neutrino telescope located in the mediterranean sea should be around 10^{-9} neutrinos $\text{cm}^{-2}\text{s}^{-1}$ for point sources in the sky. In Fig. 8 we show the central region \bar{J} skymap but calculated with a $\Delta\Omega = 10^{-3}$ resolution corresponding to the proposed km3 neutrino telescope resolution. The contour shows an optimistic benchmark region corresponding to $\bar{J} = 100$ in the zoom for GLAST (no region is available for $\bar{J} = 10^3$).

3.3.3 EGRET

A few years ago, the EGRET collaboration reported an excess in gamma ray fluxes above 1 GeV [47]. After subtracting the cosmic ray background, a residual flux of around 5×10^{-8} photons $\text{cm}^{-2}\text{s}^{-1}$ remains. The excess is hard to accommodate with natural cosmic ray propagation models, as it requires a harder electron injection spectrum or average spectrum in the galaxy different from the local ones [48]. As an alternative, the annihilation of dark matter has been suggested. To fit the energy spectrum, the dark matter candidate should have a mass around 50 GeV. With an angular resolution $\Delta\Omega = 10^{-3}$ sr (*i.e.* an opening angle of 0.1 degrees), the value of the residual flux would show as the contour on Fig. 8, when taking an optimistic HEP_γ that would correspond to $\bar{J} = 10^2$ for GLAST. The central region would indeed be observable by Egret, while the regions at higher longitudes or latitudes remain in the background. However, this is not what was observed by Egret, as the excess is found to be rather constant with latitude or longitude, except close to the galactic center region where it is mildly higher. When fitted to the data, the hypothesis of dark matter yields a structure which is incompatible with the NFW profile. Instead, an prolate isothermal halo supplemented by two rings gives good results [49]. As a consequence, a constant boost factor of order 40 is needed in this WIMP candidate scenario, and this implies excessive secondary antiprotons fluxes, in clear contradiction with observations [50]. Moreover, it has been recently argued that the EGRET excess might be due to a calibration problem rather than any unknown astrophysical or exotic contribution [51].

3.4 Sensitivity to clumps and resolution

Taken at face value, our results seem to argue that no clump in the simulation seems to be within the reach of GLAST. The intrinsic luminosity of an individual clump is determined by its mass and its concentration, but the corresponding flux is damped by the distance square factor. Inside the virial radius, the clumps contribute for 8.2% of the total luminosity for a mass fraction of 5.4%, but only for 0.2% of the total flux. This, however, depends strongly on the distance from the nearest clump. A further point to take into account is the resolution limit of the simulation. Due to that, the innermost behavior of the clumps profile is poorly determined, as already mentioned. The intrinsic luminosity of a clump can be boosted by increasing the inner slope γ . In Fig. 5c, we show the clump luminosity boost factor as a function of γ , at constant mass and concentration. For γ values less than 1.3 or 1.4 the boost factor is moderate. In particular, the boost for $\gamma = 1$ (NFW profile) compared to $\gamma = 0$ (*core*) is only around a factor of 2. However, for values of γ above 1.3 the boost factor increases very spectacularly, to reach a factor of 10 around $\gamma = 1.4$.

To have a much stronger effect, the concentration parameter should be increased. If we take a NFW profile for the clump, it is easy to check that the concentration parameter is directly expressed in terms of the scale radius a and the virial radius of the clump r_{cl} as $c_{vir} = r_{cl}/a$. Then the total annihilation

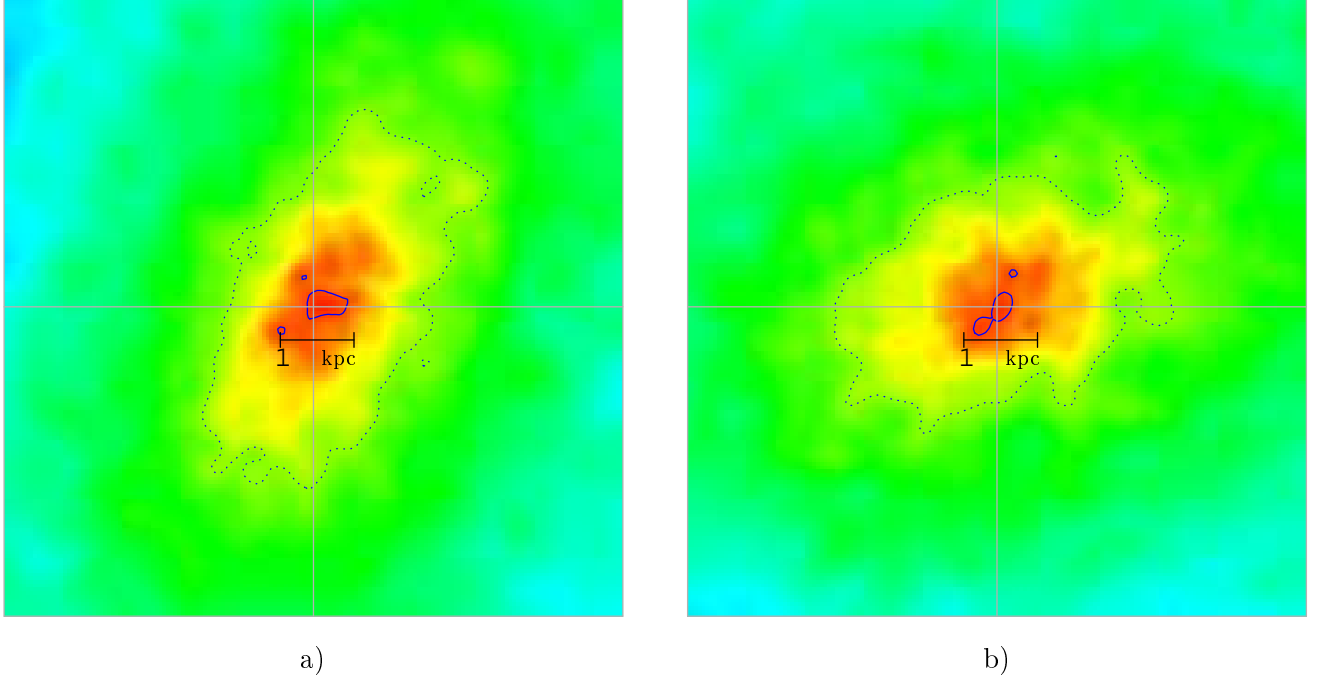


Figure 7: a) Zoom in the $60^\circ \times 60^\circ$ central region of Fig. 6, i.e. a region centered around the direction of the Galactic center. The horizontal bar gives the distance of 1 kpc, which is roughly the region which will be an interesting target for GLAST. The contours correspond to $\bar{J} = 10^3$ (solid) and $\bar{J} = 10^2$ (dotted). b) Same as a) but with observer position at $(R_{sun}, 0, 0)$ instead of $(0, 0, R_{sun})$ in a). The two plots are normalized with the same local density value.

\bar{J} resulting from a clump of virial mass M_{vir}^{cl} sitting at a distance $l \gg r_{cl}$ will be given by

$$J_{cl} \simeq \frac{4\pi}{3} \frac{r_{cl}^2}{l^2} \frac{r_{cl}}{r_0} \frac{\rho_{vir}^2}{\rho_0^2} f_{cl}(c_{vir}), \quad (11)$$

where ρ_{vir} is the virial density (200 times the cosmological matter density), and

$$f(x) = \frac{(1+x^2)^2}{x} \left(1 - \frac{1}{(1+x)^3} \right) \simeq x^3 \quad (12)$$

for $x \gg 1$. The clump mass and clump size are related by the following relation

$$M_{cl} = 4\pi \rho_{vir} r_{cl}^3 \left(\ln(1+c_{vir}) - \frac{c_{vir}}{(1+c_{vir})} \right) \quad (13)$$

From this – as $\rho_{vir}/\rho_0 \simeq 10^{-3}$ and since the probability of having a clump in our immediate neighborhood is low – we see that small (in angular size) clumps will be visible by GLAST only if they are highly concentrated, $c_{vir} \sim 10^2 - 10^3$.

4 Conclusion & Perspectives

We evaluated the gamma and neutrino fluxes from dark matter annihilation in a galactic halo framework extracted from a cosmological N-body simulation of the HORIZON project. Although such simulations are the most elaborate and realistic framework for this kind of studies, there are very few works concerning dark matter detection in N-body frameworks. With reasonable assumptions on the new

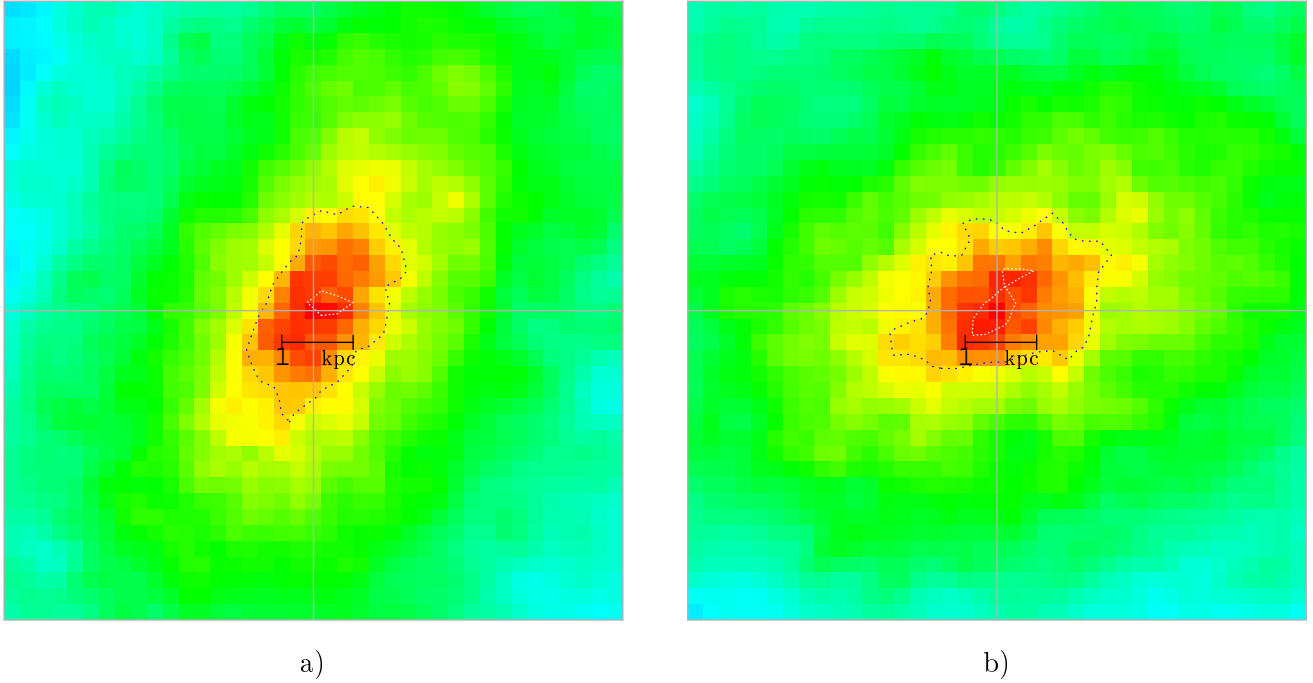


Figure 8: a) Same as figure 7 with $\Delta\Omega = 10^{-3}$ for a km³ neutrino telescope and EGRET, i.e. the $60^\circ \times 60^\circ$ region around the Galactic center of the $\bar{J}(\Delta\Omega = 10^{-3})$ skymap. The light contour corresponds to an hypothetical km³ size neutrino telescope, the dark one corresponds to the level of the controversial EGRET excess. b) Same as a) but with observer position at $(R_{sun}, 0, 0)$ instead of $(0, 0, R_{sun})$ in a). The two plots are normalized with the same local density value.

physics beyond the standard model and on the cosmological scenario for dark matter particles, we proposed an absolute evaluation of gamma and neutrino fluxes. This allowed to test the galactic simulation framework with regard to dark matter indirect detection in future experiments like GLAST and the proposed km3 size neutrino telescope in the mediterranean sea extrapolated from ANTARES sensitivity and preliminary KM3NeT studies.

Our framework and even other cosmological simulations have a resolution limit which is lower than what would be desirable for this type of studies. Nevertheless, it was possible to reach a number of interesting results in our framework. In particular, we showed that the galactic center region is a good benchmark part of the sky with regard to the GLAST sensitivity. Even if it is more challenging, this region should also be studied by future neutrino telescopes, especially a km3 size telescope. Individual clumps stand out clearer in the direction of the galactic anticenter. The concentration parameters of the clumps are then the crucial information that will determine the flux. Unfortunately, our simulation does not provide enough information on scales below 100 pc to clearly conclude about the detectability of individual subhalos. Furthermore, it should be stressed that our results for the central region of the Galaxy and for the clumps should be considered as a lower bound. A resolution improvement will increase the values of the central density and decrease the size of the central region within which we have little or no information. This will increase the signal in the direction of the Galactic center, as well as in the directions of the clumps. We can hope that specific geometry, non sphericity and structures especially in the central region will be highlighted by future gamma and neutrino observations.

Cosmological simulations made very important progress in the last few years, and a study of gamma-ray induced by dark matter annihilation in the most precise N-BODY framework can be found in [17] with a resolution allowing the identification of $\lesssim 10^6 M_{sun}$ clumps. Though the quality of this work is impressive, this minimal scale is still more than 10 orders of magnitude above the typical WIMP free-streaming scale ($\sim 10^{-12-4} M_{sun}$ [52]) and also considerably bigger than the minimal surviving clump mass, which anyway is still under debate.

Acknowledgments

We would like to thank V. Bertin, A. Bosma and J. Lavalley for helpful discussions. FSL work is supported by a FNRS belgium grant and the IAP. EN work was also partially supported by a FNRS grant. We also acknowledge the french Astroparticle Program and the grant ANR-06-BLAN-0172 for financial support.

References

- [1] D. N. Spergel et al. Wilkinson microwave anisotropy probe (wmap) three year results: Implications for cosmology. 0300.
- [2] Albert Bosma. Dark matter in galaxies: Observational overview. *Dark Matter in Galaxies, IAU symposium series*, 220, 2004.
- [3] Simon D. M. White, Carlos S. Frenk, Marc Davis, and George Efstathiou. Clusters, filaments, and voids in a universe dominated by cold dark matter. *Astrophys. J.*, 313:505–516, 1987.
- [4] Douglas Clowe, Anthony Gonzalez, and Maxim Markevitch. Weak lensing mass reconstruction of the interacting cluster 1e0657-558: Direct evidence for the existence of dark matter. *Astrophys. J.*, 604:596–603, 2004.
- [5] Ignacio Ferreras, Prasenjit Saha, and Scott Burles. Unveiling dark halos in lensing galaxies. 2007.
- [6] Gerard Jungman, Marc Kamionkowski, and Kim Griest. Supersymmetric dark matter. *Phys. Rept.*, 267:195–373, 1996.
- [7] Gianfranco Bertone, Dan Hooper, and Joseph Silk. Particle dark matter: Evidence, candidates and constraints. *Phys. Rept.*, 405:279–390, 2005.
- [8] E. Athanassoula. Bars and the connection between dark and visible matter. 2003.

- [9] Brandon Allgood, Ricardo A. Flores, Joel R. Primack, Andrey V. Kravtsov, Risa H. Wechsler, Andreas Faltenbacher, and James S. Bullock. The shape of dark matter haloes: dependence on mass, redshift, radius and formation. *Mon. Not. Roy. Astron. Soc.*, 367:1781–1796, 2006.
- [10] E. Athanassoula. A bar in the inner halo of barred galaxies i. structure and kinematics of a representative model. *Mon. Not. Roy. Astron. Soc.*, 377:1569–1578, 2007.
- [11] Clayton Heller, Isaac Shlosman, and E. Athanassoula. Structure formation inside triaxial dark matter halos: Galactic disks, bulges and bars. 2007.
- [12] Julio F. Navarro, Carlos S. Frenk, and Simon D. M. White. A universal density profile from hierarchical clustering. *Astrophys. J.*, 490:493–508, 1997.
- [13] Andrey V. Kravtsov, Anatoly A. Klypin, James S. Bullock, and Joel R. Primack. The cores of dark matter dominated galaxies: theory vs. observations. *Astrophys. J.*, 502:48, 1998.
- [14] Ben Moore, Tom Quinn, Fabio Governato, Joachim Stadel, and George Lake. Cold collapse and the core catastrophe. *Mon. Not. Roy. Astron. Soc.*, 310:1147–1152, 1999.
- [15] Felix Stoehr, Simon D. M. White, Volker Springel, Giuseppe Tormen, and Naoki Yoshida. Dark matter annihilation in the milky way’s halo. *Mon. Not. Roy. Astron. Soc.*, 345:1313, 2003.
- [16] Jurg Diemand, Michael Kuhlen, and Piero Madau. Dark matter substructure and gamma-ray annihilation in the milky way halo. *Astrophys. J.*, 657:262, 2007.
- [17] Michael Kuhlen, Jurg Diemand, and Piero Madau. Glast and dark matter substructure in the milky way. *AIP Conf. Proc.*, 921:135–138, 2007.
- [18] Michael Kuhlen, Jurg Diemand, and Piero Madau. The Dark Matter Annihilation Signal from Galactic Substructure: Predictions for GLAST. 2008.
- [19] Argyro Tasitsiomi and A. V. Olinto. The detectability of neutralino clumps via atmospheric cherenkov telescopes. *Phys. Rev.*, D66:083006, 2002.
- [20] Lidia Pieri and Enzo Branchini. On dark matter annihilation in the local group. *Phys. Rev.*, D69:043512, 2004.
- [21] Savvas M. Koushiappas, Andrew R. Zentner, and Terrence P. Walker. The observability of gamma-rays from neutralino annihilations in milky way substructure. *Phys. Rev.*, D69:043501, 2004.
- [22] Xiao-Jun Bi. Gamma rays from the neutralino dark matter annihilations in the milky way substructures. *Nucl. Phys.*, B741:83–107, 2006.
- [23] L. Pieri, G. Bertone, and E Branchini. Dark matter annihilation in substructures revised. 2007.
- [24] N. W. Evans, F. Ferrer, and Subir Sarkar. A ‘Baedeker’ for the dark matter annihilation signal. *Phys. Rev.*, D69:123501, 2004.
- [25] Lidia Pieri, Enzo Branchini, and Stefan Hofmann. Difficulty of detecting minihalos via gamm rays from dark matter annihilation. *Phys. Rev. Lett.*, 95:211301, 2005.
- [26] Takeshi Oda, Tomonori Totani, and Masahiro Nagashima. Gamma-ray background from neutralino annihilation in the first cosmological objects. *Astrophys. J.*, 633:L65–L68, 2005.
- [27] Savvas M. Koushiappas. Proper motion of gamma-rays from microhalo sources. *Phys. Rev. Lett.*, 97:191301, 2006.
- [28] Edward A. Baltz, James E. Taylor, and Lawrence L. Wai. Can astrophysical gamma ray sources mimic dark matter annihilation in galactic satellites? 2006.
- [29] Louis E. Strigari, Savvas M. Koushiappas, James S. Bullock, and Manoj Kaplinghat. Precise constraints on the dark matter content of Milky Way dwarf galaxies for gamma-ray experiments. *Phys. Rev.*, D75:083526, 2007.
- [30] Louis E. Strigari et al. The Most Dark Matter Dominated Galaxies: Predicted Gamma- ray Signals from the Faintest Milky Way Dwarfs. 2007.
- [31] The horizon project, <http://www.projet-horizon.fr>.
- [32] R. Teyssier. Cosmological hydrodynamics with adaptive mesh refinement. a new high resolution code called ramses. *A&A*, 385:337–364, 2002.

- [33] S. Casertano and P. Hut. Core radius and density measurements in N-body experiments Connections with theoretical and observational definitions. *APJ*, 298:80–94, November 1985.
- [34] Dominique Aubert, Christophe Pichon, and Stephane Colombi. The origin and implications of dark matter anisotropic cosmic infall on l^* haloes. *Mon. Not. Roy. Astron. Soc.*, 352:376, 2004.
- [35] Matthias Bailin, Jeremy; Steinmetz. Internal and External Alignment of the Shapes and Angular Momenta of LCDM Halos. *Astrophys. J.*, 627:647–665, 2005.
- [36] B. et al. Allgood. The shape of dark matter haloes: dependence on mass, redshift, radius and formation. *MNRAS*, 367:1781–1796, 2006.
- [37] Torbjorn Sjostrand, Stephen Mrenna, and Peter Skands. PYTHIA 6.4 physics and manual. *JHEP*, 05:026, 2006.
- [38] Y. Mambrini, C. Munoz, E. Nezri, and F. Prada. Adiabatic compression and indirect detection of supersymmetric dark matter. *JCAP*, 0601:010, 2006.
- [39] Benjamin Labonne, Emmanuel Nezri, and Jean Orloff. The suppression of neutralino annihilation into $Z h$. *Eur. Phys. J.*, C47:805–814, 2006.
- [40] Gianfranco Bertone, Emmanuel Nezri, Jean Orloff, and Joseph Silk. Neutrinos from dark matter annihilations at the galactic centre. *Phys. Rev.*, D70:063503, 2004.
- [41] Marc Kamionkowski and Savvas M. Koushiappas. Galactic substructure and direct detection of dark matter. arXiv:0801.3269 [astro-ph].
- [42] N. Gehrels and P. Michelson. Glast: The next-generation high energy gamma-ray astronomy mission. *Astropart. Phys.*, 11:277–282, 1999.
- [43] Gianfranco Bertone, Torsten Bringmann, Riccardo Rando, Giovanni Busetto, and Aldo Morselli. Glast sensitivity to point sources of dark matter annihilation. astro-ph/0612387.
- [44] J. Carr et al. Sensitivity studies for the cubic-kilometre deep-sea neutrino telescope KM3NeT. Proceedings of 30th International Cosmic Ray Conference (ICRC 2007), Merida, Yucatan, Mexico, 3-11 Jul 2007. arXiv:0711.2145 [astro-ph].
- [45] D. Bailey. *Monte Carlo tools and analysis methods for understanding the ANTARES experiment and predicting its sensitivity to Dark Matter*. Ph.D. thesis 2002, <http://antares.in2p3.fr/Publications/thesis/2002/d-bailey-thesis.ps.gz>.
- [46] Gordon Lim. Indirect search for Dark Matter with the ANTARES neutrino telescope. Proceedings of 15th International Conference on Supersymmetry and the Unification of Fundamental Interactions (SUSY07), Karlsruhe, Germany, 26 Jul - 1 Aug 2007. arXiv:0710.3685 [astro-ph].
- [47] S.D. et al. Hunter. Egret observations of the diffuse gamma ray emission from the galactic plane. *The Astrophysical Journal*, 481(1):205–240, 1997.
- [48] Andrew W. Strong, Igor V. Moskalenko, and Olaf Reimer. Diffuse Galactic continuum gamma rays. A model compatible with EGRET data and cosmic-ray measurements. *Astrophys. J.*, 613:962–976, 2004.
- [49] Wim de Boer, C. Sander, V. Zhukov, A. V. Gladyshev, and D. I. Kazakov. EGRET excess of diffuse galactic gamma rays interpreted as a signal of dark matter annihilation. *Phys. Rev. Lett.*, 95:209001, 2005.
- [50] L. Bergstrom, J. Edsjo, Michael Gustafsson, and P. Salati. Is the dark matter interpretation of the EGRET gamma excess compatible with antiproton measurements? *JCAP*, 0605:006, 2006.
- [51] F. W. Stecker, S. D. Hunter, and D. A. Kniffen. The Likely Cause of the EGRET GeV Anomaly and its Implications. *Astropart. Phys.*, 29:25–29, 2008.
- [52] S. Profumo, K. Sigurdson, and M. Kamionkowski. What Mass Are the Smallest Protohalos? *Physical Review Letters*, 97(3):031301, July 2006.